CHALMERS
UNIVERSITY OF TECHNOLOGY

Experimental study-based hybrid SVR-GWO modeling of copper sustainable reclamation from spent printed circuit boards (PCBs) induced

Citation for the original published paper (version of record):
Shakib, B., Kang, H., Khiadani, M. et al (2024). Experimental study-based hybrid SVR-GWO modeling of copper sustainable reclamation from spent
printed circuit boards (PCBs) induced by leaching followed by liquid–liquid extraction. Journal of Environmental Chemical Engineering, 12(5). http://dx.doi.org/10.1016/j.jece.2024.114056

Journal of Environmental Chemical Engineering 12 (2024) 114056

Contents lists available at ScienceDirect

Journal of Environmental Chemical Engineering

journal homepage: www.elsevier.com/locate/jece

Experimental study-based hybrid SVR-GWO modeling of copper sustainable reclamation from spent printed circuit boards (PCBs) induced by leaching followed by liquid–liquid extraction

Benyamin Shakib [a,b], Hee-Nam Kang [a], Mehdi Khiadani [c,d], Martina Petranikova [e], Rajesh Kumar Jyothi [f], Amir Razmjou [c,d], Jin-Young Lee [a,b,*]

[a] Resources Utilization Research Division, Korea Institute of Geoscience and Mineral Resources (KIGAM), 124 Gwahak-ro, Yuseong-gu, Daejeon 34132, Republic of Korea
[b] Department of Resources Engineering, Korea University of Science and Technology (UST), 217 Gajeong-ro, Yuseong-gu, Daejeon 34113, Republic of Korea
[c] School of Engineering, Edith Cowan University, 270 Joondalup Drive, Joondalup, Perth, WA 6027, Australia
[d] Mineral Recovery Research Center (MRRC), School of Engineering, Edith Cowan University, Joondalup, Perth, WA 6027, Australia
[e] Department of Chemistry and Chemical Engineering, Chalmers University of Technology, Kemivägen 4, Gothenburg SE-41296, Sweden
[f] CSIRO Mineral Resources (CMR), Australian Mineral Research Center (AMRC), 7 Conlon St. Waterford, Perth, WA 6102, Australia

ARTICLE INFO

Keywords:
Spent PCBs
Copper
Recycling
Leaching
Uncertainty
SVR model

ABSTRACT

Reclamation of copper from waste printed circuit boards (WPCBs) is critical in advancing eco-friendly manufacturing methods by considering viable secondary metal resources. Herein, this study introduced a novel hybrid intelligence model that relies on a support vector regression–grey wolf optimization (SVR-GWO) approach to predict, validate, and optimize the leaching of WPCBs in nitrate solution and copper purification using LIX 973 N. The hybrid model's performance surpassed that of the standalone SVR model due to fine-tuning hyperparameters using the GWO approach, as indicated by the lower values of MSE and narrow error distribution in the leaching, extraction, and stripping experiments. The modeling data indicated that 96.1 % of the copper in the WPCB material was dissolved during leaching at 75°C, using a pulp density of 7 % for 2 h. During the extraction phase, the hybrid model optimized the structure performance of equilibrium pH, extractant concentration, contact time, and O/A ratio, resulting in values of 2.5, 30 %, 20 min, and 1, respectively. The predicted isotherm data for the McCabe-Thiele diagram, derived from the developed model, suggested four operational stages for extracting copper from the leach solution. Under optimized conditions of 2 M H_2SO_4 and 0.3 A/O phase ratio at 25 °C for 20 min, the complete stripping process from the loaded organic phase required applying three counter-current stages. These developments highlight the capability of the SVR-GWO method to improve copper extraction from WPCBs, thereby making a substantial contribution to sustainable recycling efforts.

1. Introduction

Worldwide, the demand and production for electrical and electronic equipment (EEE) are increasing fast, which leads to the creation of electronic waste (e-waste) [1]. Discarded printed circuit boards (PCBs) represent a significant portion of e-waste, with waste PCBs (WPCBs) comprising approximately 3–6 % of the total e-waste by weight [2]. Currently, the predominant disposal method for PCBs involves incineration or deposition in landfills, resulting in adverse environmental impacts associated with generating toxic chemicals such as dioxins, furans, and other hazardous substances [3]. The foundational structure of PCBs serves as the electronic infrastructure of the device, with copper being the primary conducting material. The quantity of copper in PCBs can vary based on the number of layers and the level of electricity it is designed to handle [4]. Typically, it accounts for approximately 15–35 % of the overall weight of the PCB [5]. Copper, an essential element for the health of humans and organisms, has raised concerns for the ecosystem because of increased environmental exposure resulting from human activities [6]. An increased amount of Cu in the water can lead to protein inactivation and damage to the natural defense system

* Corresponding author at: Resources Utilization Research Division, Korea Institute of Geoscience and Mineral Resources (KIGAM), 124 Gwahak-ro, Yuseong-gu, Daejeon 34132, Republic of Korea.
E-mail addresses: b.shakib@kigam.re.kr, benyamin@ust.ac.kr (B. Shakib), martina.petranikova@chalmers.se (M. Petranikova), jinlee@kigam.re.kr (J.-Y. Lee).

https://doi.org/10.1016/j.jece.2024.114056
Received 25 June 2024; Received in revised form 7 August 2024; Accepted 3 September 2024
Available online 4 September 2024

against oxidation. This can disrupt metabolic processes and hinder the growth of aquatic organisms [7]. It is imperative to emphasize the importance of effectively recycling WPCBs, as this practice holds considerable environmental importance. Moreover, Cu plays a crucial role in facilitating the shift towards a more sustainable future due to its widespread use as a conductor and its significant pertinence to virtually every industry. Also, the depletion of Cu resources necessitates the sustainable recovery of the metal from secondary sources.

The recent literature reviews have discussed the findings of researchers who have conducted studies on the recycling process of WPCBs using hydro-, pyro-, and bio-metallurgical methods [8,9]. High temperatures are involved in the pyro-metallurgy process, and they are linked to several disadvantages, such as the depletion of noble metals into slag, the production of substantial quantities of gaseous emissions, and the limited retrieval of other metallic elements [10]. Microorganisms in bio-metallurgical processes break down metals, but despite being environmentally friendly, this process is slow and doesn't always result in complete metal recovery [11]. Conversely, the hydro-metallurgy technique demonstrates comparatively lower initial investment expenses, limited atmospheric pollution concerns, and superior specificity in metals retrieval [12]. The first step in this method is preparing the discarded end-of-life PCBs for treatment, followed by leaching, separation, and purification processes [13].

One commonly used method for separating base metals involves using aqueous acids like sulfuric or hydrochloric acid for leaching experiments. Combining acids with an oxidizing agent is essential when attempting to recover metals from WPCBs, as the metals in the electronic boards exist in their pure elemental states. Appropriate oxidizing agents for leaching reactions include hydrogen peroxide, chlorine gas, oxygen, bacteria, or nitric acid [14,15]. So far, several researchers have reported the procedures for removing and intensifying valuable metals from exhausted PCB solutions. Oh and co-workers observed that using a mixture of 2 M H_2SO_4 with 0.2 M H_2O_2 as an oxidizing agent, Cu leaching from WPCBs exceeded 95 % after being heated at 85 °C for 12 h, which there was also a reported simultaneous dissolution of Ni, Al, Zn, and Fe [16]. Rao and co-workers have suggested two stages of an oxidative leaching technique for retrieving Cu and Au from outdated mobile phone PCBs, yielding a metal composition containing 84 % Cu and 0.05 % Au [17]. Subsequently, purification process solutions were acquired using liquid-liquid extraction, wherein Cu was extracted using a diluted phenolic oxime extractant in kerosene. Yang and co-workers analyzed the impact of operational parameters on the separation of Cu from WPCBs, looking at operating variables like H_2SO_4 concentration, H_2O_2 dosage, particle size, cupric ions presence, reaction temperature, and contact duration in the leaching process [18]. The optimal condition for leaching 10 g of waste powder with a pulp density of 10 % for 3 h at ambient temperature was to combine 100 ML of 15 % H_2SO_4 with 10 ML of 30 % H_2O_2. In a similar study, Birloaga and co-workers reported on Cu and Au recovery when they examined how adjusting the H_2SO_4 concentration, H_2O_2 addition, temperature, stirring rate, and leaching time affected the results [19]. Kumar and co-workers conducted a comparative analysis of the efficacy of nitric acid and a sulfuric acid/hydrogen peroxide mixture in the leaching of Cu from WPCBs [20]. Experimental results revealed that under the experimental conditions of a pulp density of 100 g/L and a temperature of 90°C for 5 h, 3 M HNO_3 leached 96 % of the copper. In contrast, the mixture of 1.2 M H_2SO_4 and 10 % H_2O_2 facilitated the leaching of 75.7 % copper with the equivalent pulp density at 50°C for 4 h.

The extensive array of conditions documented in existing literature necessitates the utilization of a methodology capable of evaluating the specific influence of each process circumstance on total efficacy in undertaking the task of process optimization. Nowadays, machine learning (ML) models have gained considerable prominence across multiple sectors as significant focus is directed toward leveraging this technology to enhance diverse processes [21,22]. The utility of this methodology is primarily evident in its ability to facilitate data analysis within a framework that enables the assessment of the impact of various inputs believed to influence a specific response. A literature review reveals various investigations on applying artificial intelligence (AI) techniques to model and optimize reactive extraction systems. Table 1 provides an overview of some of these studies.

Support vector regression (SVR) is a well-established machine learning technique that has demonstrated efficacy across various disciplines and domains. Despite its widespread application, SVR has not been utilized for predictive capability evaluation of leaching and liquid–liquid extraction. Notwithstanding the SVR advantages, optimizing its parameters demands meticulous adjustment of hyperparameters, a process characterized by substantial computational requirements. To address this issue, the Grey Wolf Optimization (GWO) algorithm, a meta-heuristic optimization technique founded on grey wolf social hierarchy and hunting behaviors, was utilized to improve the precision of the model. The integrated SVR-GWO approach proficiently addresses the intricate interactions and non-linear relationships among various factors that affect the leaching and extraction processes, which is essential for enhancing the recovery of copper from waste printed circuit boards (WPCBs). Also, a thorough uncertainty assessment was carried out through stochastic simulation to address the intrinsic uncertainties associated with copper separation from WPCBs in the process parameters, improving the reliability of the predictive model.

Previous research on the separation of copper from WPCBs has not adequately addressed the interactive relationships among the variables that affect the results, nor has it incorporated uncertainty analysis, performance prediction, selectivity enhancement, or structural

Table 1
Summary of some recent studies on modeling reactive extraction systems using machine learning algorithms.

AI methods	Goals	Studied parameters	Recovery rate	Ref
ANN-GA	Extraction of Ce with Cyanex 572	pH, Cyanex 572 concentration, nitrate ion concentration, and contact time	95.2 % cerium	[42]
ANN-PSO	Cu removal with ZVI/rGO magnetic nanocomposites	Temperature, initial pH, initial concentration, and contact time	87.2 % copper	[43]
ANN-GA	Extraction of $C_4H_6O_6$ with Amberlite LA−2	Tartaric acid concentration, pH, and amine concentration	96.1 % tartaric acid	[44]
ANN-GA	Ferulago angulate extraction with super critical carbon dioxide	Pressure, temperature, particle size, and dynamic time	86.3 % essential oil	[45]
ANN	Sulfate removal with chemical precipitation	Temperature, $BaCl_2$ dosage, and mixing speed	99.5 % Sulfate	[46]
ANN	Removal of Ni and Co with ion exchange	pH, initial concentration, clinoptilolite dosage, particle size, and temperature	92.8 % Ni and 33.6 % Co	[47]
ANN	Extraction of Fe and Zn with LIX 984 N and D2EHPA	pH, temperature, and extractants concentration	99.1 % Fe and 4.5 % Zn	[48]
SVR	Cr removal with biosorption process	Contact time, sorbate concentration, pH, and temperature	~14 mg/g sorption capacity	[49]
ANFIS	Cu leaching with sulfuric acid	Time, pH, Cu and Fe concentration	92.6 % Cu	[50]
ANFIS	Cu adsorption with Clinoptilolite	Initial pH, adsorbent dosage, contact time	93.6 % Cu	[51]
ANFIS	Cr adsorption with cellulose nanocrystals and sodium alginate	Contact time, adsorbent dosage, Cr concentration, and pH	350.23 mg/g sorption capacity	[52]

optimization. Consequently, the present study represents the novel application of a hybrid hydrometallurgical approach for separating copper from WPCBs by integrating the developed ML model with Monte Carlo simulation (MCS) techniques. To this end, a series of experiments on Cu leaching and liquid–liquid extraction were conducted and used to train and validate the applied model. The optimized hybrid model-based experimental data allowed for a detailed study of Cu sustainable separation from WPCBs, validation, prediction, leaching kinetics, necessary counter-current stages, and the risk analysis associated with operational parameters.

2. Experimental and modeling methods

2.1. Materials

Scrap PCBs were obtained from a local computer recycling company in Daejeon, Republic of Korea, and subjected to pre-treatment. Initially, the scrap underwent heat treatment on the back side of the PCB to eliminate small components. Moreover, the flat PCBs were segmented into smaller units with dimensions of 7×7 cm and subsequently processed through a shredding mechanism to reduce their sizes to 2×2 mm. The solid samples were assembled and dissolved in aqua regia by considering replicates two times to analyze and confirm the metal content using HNO_3 (60 % purity) and HCl (35 % purity) obtained from Junsei Chemical Co., Ltd. The processed sample of powdered WPCBs was characterized by its composition of 35.6 wt% Cu, 1.1 wt% Al, 0.7 wt % Fe, 0.4 wt% Ni, 1.2 wt% Sn, 0.2 wt% Pb, and 60.8 wt% epoxy resins and ceramics. Kerosene (95 % purity), supplied by Samchun Chemical Co., Ltd., with a boiling point range of 180–270 °C, was employed as a diluent in the organic phase preparation. The chelating extractant LIX 973 N, a mixture of 5-dodecyl-salicylaldoxime and 2-hydroxy-5-nonylacetophenone oxime, procured from Cognis Ireland Ltd., was employed for Cu separation from the leach solution in combination with 5 %(v/v) 1-Decanol obtained from Alfa Aesar Co., which served as a modifier. The 99.0 % pure TBP extractant provided by Samchun Chemical Co., Ltd. was used to treat the leach liquor of WPCBs to recycle and recover HNO_3. Also, H_2SO_4 (95.0 %, Samchun Chemical Co., Ltd.) and NH_4OH (26.0 %, Daejung Chemicals Co., Ltd.) were employed to modulate the pH levels of solutions. All employed chemical materials were in their as-received state without undergoing additional purification processes.

2.2. Analysis methods

The pH of the aqueous solution was determined using a digital pH meter (Thermo Scientific Orion 3-Star model) equipped with a combined glass electrode. The concentration of metal ions in the aqueous phase was quantified using an ICP-OES, specifically the PerkinElmer Optima 8300 model. Also, a mechanical shaker (SI 600 R Refrigerated Incubator) was employed for phases mixing to achieve equilibrium during the liquid–liquid extraction phase. Fourier Transform Infrared Spectroscopy (FTIR) was employed to analyze the characteristics of the organic phases, utilizing a Thermo Scientific Nicolet 6700 model. The characterization and analysis of the crystal structure of the material was investigated using an X-ray diffractometer (XRD) equipped with a PHILLIPS X′pert MPD instrument, and the observable morphology of the final sample was examined utilizing a scanning electron microscope (SEM) model Merlin Compact from Carl Zeiss in Germany.

2.3. Experiment procedure

The obtained WPCBs from the pre-processing stage were utilized for all leaching studies in 100 ML flat-bottomed three-neck glass flasks connected to a water bath. In the leaching procedure, intensified HNO_3 concentrations led to substantial quantities of NO_x gases. Thus, a fully jacketed scrubber was implemented to manage the system effectively, and a water-cooled condenser was employed to capture and disperse the induced heat during the gas condensation [23]. HNO_3 concentration was pre-adjusted with deionized water and then maintained at a specified temperature range of 15–75 °C for a predetermined leaching time. During the leaching tests, the process was agitated at a consistent speed of 700 rpm, and periodic samples of the resulting leach liquor solution were obtained and subsequently diluted to a predetermined volume for ICP-OES analysis. In each stage, the effectiveness of metal leaching was evaluated from:

$$L(\%) = \frac{C_1 V_1}{C_1 V_1 + C_2 V_2} \times 100 \tag{1}$$

where the variables C_1 and C_2 denote the concentrations of metals in the leaching solution and filter residue solution, expressed in mg/L units. V_1 and V_2 denote the measured volumes of the leaching solution and filter residue solution in liters. The bench-scale for extraction and stripping experiments involved the combination of equal volumes (10 ML) of leach liquor and organic extractant, excluding A/O ratio experiments, utilizing a mechanical shaker for mixing. Once the designated time had elapsed, the liquids' mixture was relocated to a decanter to enable the process of settling and separation. The determination of extraction and stripping percentages was performed using the following calculations:

$$E(\%) = \frac{[M]_t - [M]_{aq}}{[M]_t} \times 100 \tag{2}$$

$$S(\%) = \frac{[M]_{aq,a}}{[M]_{org,t}} \times 100 \tag{3}$$

The variables $[M]_t$ and $[M]_{aq}$ denote the concentrations of the metal ions in the feed solution and final aqueous phase, respectively. Additionally, the symbol $[M]_{aq,a}$ represents the equilibrium concentration of metal ions in the stripping solution, while $[M]_{org,t}$ denotes the initial concentration of the metal ion in the loaded organic phase.

2.4. Support vector regression (SVR) model

SVR is a widely utilized the machine learning algorithm (MLA) derived from the concept formulated by Vapnik [24]. This approach is grounded in the statistical learning theory, which involves the concept of structural risk minimization. The utilization of this method is proven to be highly effective for both linear and non-linear classification, in addition to its efficacy in addressing non-linear regression challenges. The connection of the non-linear concept of SVR can be articulated as demonstrated below [25]:

$$Min \frac{1}{2}||\nu||^2 + P\sum_{i=1}^{N}(\xi_i + \xi_i^*) subject\ to \begin{cases} y_b - (\nu \varnothing(z_b) + c_b) \le \varepsilon + \xi_b \\ (\nu\phi(z_b) + c_b) - y_b \le \varepsilon + \xi_b^* \\ \xi_b, \xi_b^* \ge 0 \end{cases} \tag{4}$$

The penalty parameter, denoted as P, serves to reconcile the empirical risk and model flatness, while the variables ξ_b and ξ_b^* are slack factors. Additionally, the constant ε, referred to as the tube size, embodies the optimization implementation [26]. The issue of dual convex optimization, as defined by Eq. (1), is addressed by the employment of the Lagrangian function:

$$L(\nu, c, \xi_b, \xi_b^*, \beta_b, \beta_b^*, \delta_b, \delta_b^*) = \frac{1}{2}||\nu||^2 + D\sum_{b=1}^{l}\xi_b + \xi_b^* - \sum_{b=1}^{l}\beta_b(\xi_b + \varepsilon - y_b + \nu\phi(z_b) + c) - \sum_{b=1}^{l}\beta_b^*(\xi_b^* + \varepsilon + y_b - \nu\phi(z_b) - c) - \sum_{b=1}^{l}(\delta_b\xi_b + \delta_b^*\xi_b^*) \quad (5)$$

The Lagrangian multipliers δ_b, δ_b^*, β_b, and β_b^* were denoted in the given context. The regression function of the SVR algorithm was subsequently computed in the following manner [27]:

$$k(z) = \sum_{b=1}^{l}(\beta_b - \beta_b^*)m(z, z_b) + c \quad (6)$$

The kernel function $m(z, z_b)$ and the dual variables β_b and β_b^* are significant components in this scenario. The utilization of the radial basis function (RBF) kernel was derived from the following equation to assess its performance in the analysis.

$$m(z, z_b) = \exp\left(-\gamma||z - z_b||^2\right) \quad (7)$$

The parameter γ denotes the kernel function and the selection of the values for P and γ is of great significance in achieving optimal results.

2.5. Grey wolf optimizer (GWO) algorithm

The GWO algorithm is a meta-heuristic optimization technique that was devised through the emulation of the social hierarchy and hunting behavior exhibited by gray wolves [28]. The hierarchical structure of leadership is exemplified in this study through the use of four distinct categories of wolves: alpha [α], beta [β], delta [δ], and omega [ω]. Moreover, the simulation of wolves' predatory behavior involves locating, pursuing, and surrounding prey before initiating an attack [29]. The α-wolves are situated at the apex of the social hierarchy and are responsible for making decisions, with other wolves subsequently adhering to their leadership. The β-wolves assist the alpha members of their pack and collaborate with them to develop strategies. The δ-wolves are positioned hierarchically above other wolves and adhere to the authority of the α- and β-wolves. Ultimately, the ω-wolves are required to adhere to the regulations imposed on them [30]. The phenomenon of encircling behavior is subsequently initiated and demonstrated in the following manner:

$$\vec{D} = \left|\vec{C}.\vec{X}_p - \vec{X}_{(t)}\right| \quad \vec{C} = 2.\vec{r}_2 \quad (8)$$

$$\vec{X}(+1) = \vec{X}_p - \vec{A}.\vec{D} \quad \vec{A} = 2\vec{a}.\vec{r}_1 - \vec{a} \quad (9)$$

where the position vectors $\vec{X}$ and $\vec{X}_p$ represent the location of a gray wolf and its prey, respectively. The variable t denotes the current iteration, while the coefficient vectors $\vec{C}$ and $\vec{A}$ are also involved. Notably, the random vectors $\vec{r}_1$ and $\vec{r}_2$ are constrained to the interval [0,1]. In the act of hunting, the three optimal solutions (α, β, and δ) are utilized to approximate the position of the prey, with the resulting location being recorded. Subsequently, the remaining wolves are required to adjust their positions randomly in the vicinity of the prey:

$$\vec{D}_\alpha = \left|\vec{C}_1.\vec{X}_\alpha(t) - \vec{X}(t)\right|, \quad \vec{D}_\beta = \left|\vec{C}_2.\vec{X}_\beta(t) - \vec{X}(t)\right|, \quad \vec{D}_\delta = \left|\vec{C}_3.\vec{X}_\delta(t) - \vec{X}(t)\right| \quad (10)$$

$$\vec{X}_1(t) = \vec{X}_\alpha(t) - \vec{A}_1.\vec{D}_\alpha, \quad \vec{X}_2(t) = \vec{X}_\beta(t) - \vec{A}_2.\vec{D}_\beta, \quad \vec{X}_3(t) = \vec{X}_\delta(t) - \vec{A}_3.\vec{D}_\delta \quad (11)$$

$$\vec{X}(t+1) = \frac{\vec{X}_1(t) + \vec{X}_2(t) + \vec{X}_3(t)}{3} \quad (12)$$

2.6. Performance assessment

The variation in process variables and the unequal sizes of some variables may affect the model's suitability negatively. Input values are regularized to 0–1 to avoid computational problems using:

$$X_n = \frac{X - X_{\min}}{X_{\max} - X_{\min}} \quad (13)$$

where the variable X_n is the normalized value, with X, X_{min}, and X_{max} denoting the raw, minimum, and maximum values, respectively. The predictive accuracy of the models was determined by analyzing their absolute-average deviation (AAD), mean-squared error (MSE), root-mean-squared error (RMSE), and coefficient of determination (R^2) values. Their calculations are conducted as follows, wherein a lower AAD and a higher R^2 value indicate superior model performance.

$$AAD = \frac{1}{NDP}\sum_{i=1}^{NDP}\frac{\left|Y_i^{\exp} - Y_i^{pred}\right|}{Y_i^{\exp}} \quad (14)$$

$$MSE = \frac{1}{NDP}\sum_{i=1}^{NDP}\left(Y_i^{pred} - Y_i^{\exp}\right)^2 \quad (15)$$

$$RMSE = \sqrt{\frac{1}{NDP}\sum_{i=1}^{NDP}\left(Y_i^{pred} - Y_i^{\exp}\right)^2} \quad (16)$$

$$R^2 = 1 - \frac{\sum_{i=1}^{NDP}\left(Y_i^{pred} - Y_i^{\exp}\right)^2}{\sum_{i=1}^{NDP}\left(Y_i^{pred} - \overline{Y}^{\exp}\right)^2} \quad (17)$$

The NDP refers to the numerical values of the data points.

2.7. Model development

The machine learning-based SVR-GWO model can be deconstructed into several sequential steps. These steps include identifying target variables and selecting relevant input parameters, partitioning the data into training and testing subsets, optimizing model inputs, validating the model's performance, and assessing the predicted data. Fig. 1 depicts a comprehensive flowchart delineating the modeling process on Cu reclamation from WPCBs, providing more in-depth details about the procedure.

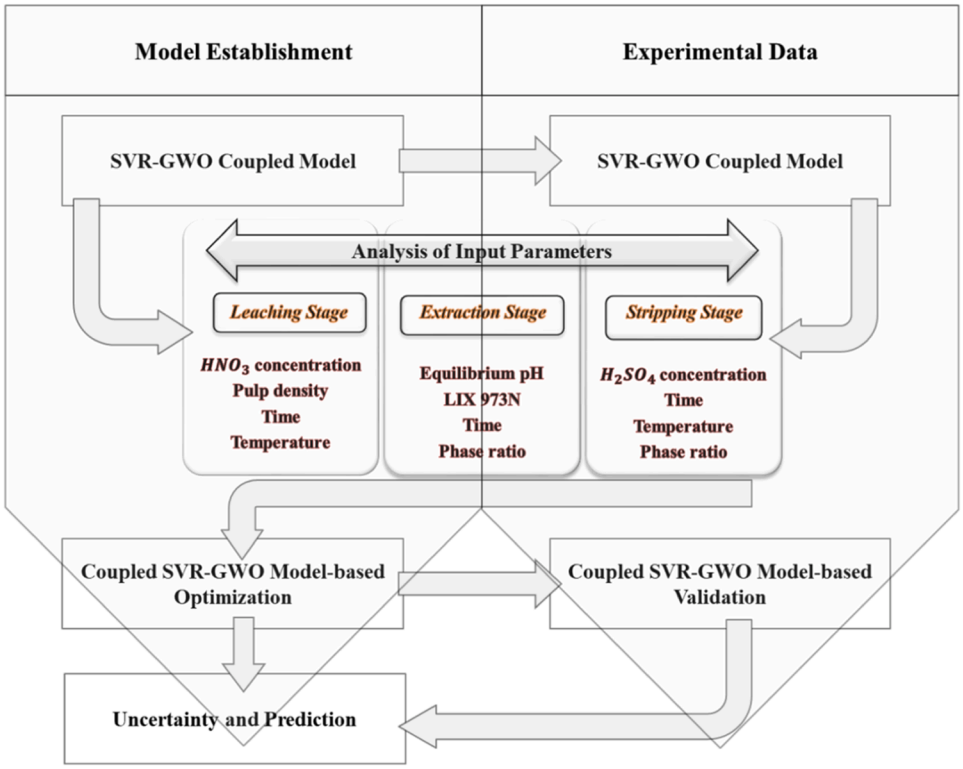

Fig. 1. Schematic processing steps presented in the copper reclamation from WPCBs.

3. Results and discussion

3.1. Development of ML models

The leaching performance involved analyzing input parameters used in the SVR and its hybrid model, focusing on HNO_3 concentration, pulp density, time, and temperature. The output of interest in these experiments was the target's leaching efficiency. A randomly selected sample of 176 data points, constituting 80 % of the total dataset, was utilized for training the developed model on Cu leaching from WPCBs. The remaining 20 % of the data, consisting of 44 data points, was reserved for validating the model's performance. In the optimization measures evaluation, it is imperative to assess their efficacy to identify the most optimal model and the meta-heuristic algorithms' usefulness for the given task. Fig S1 (a) presents the predictive accuracy of two models on the Cu leaching training dataset, with the hybrid SVR-GWO model demonstrating MSE and RMSE values of 14.6 and 7.70, respectively. The results of the models' performance on the target variable are depicted in Fig. 2(a), presenting the corresponding targets and outputs of both models' validation data sets. Fig. 2(b) displays the MSE and RMSE values for the standalone SVR and its hybrid model for the validation phase. The standalone model's MSE, RMSE, and R^2 values were 19.49, 4.41, and 0.96, while the corresponding values for the hybrid approach were 9.89, 3.14, and 0.98. Results show that the meta-heuristic coupled algorithm of SVR-GWO outperformed the SVR model due to the optimization of search parameters. Likewise, in Fig. 2(c), the dataset employed for validation sets exhibited a similar trend in the frequency of errors.

Fig. 3 shows the model predictions of Cu extraction from the leach solution, encompassing the validation data and the corresponding error values. The process optimization involved modeling the extraction parameters, including equilibrium pH, extractant concentration, duration, and O/A ratio, to consider their impact on Cu separation from the leach liquor. The 90 experimental runs were divided randomly into two sets: 80 %, or 72 runs, were allocated for training data, while the remaining 20 %, or 18 runs, were designated for validation purposes. For model training, the SVR model demonstrates an MSE value of 21.62 in Fig S1 (b), and the hybrid model exhibits a learning performance for Cu extraction from the leach solution with an MSE value of 2.55, emphasizing its improved accuracy and efficiency. Fig. 3(a) depict the objectives and results of the validation set for models, illustrating the effectiveness of the combined model's output with Cu extraction. Based on Fig. 3(b), the examination of the MSE and RMSE outcomes demonstrates that during the validation phase, the hybridized approach exhibits the lowest level of error (MSE=6.25 and RMSE=2.50) when compared to the standalone SVR algorithm (MSE=34.16 and RMSE=5.84). Moreover, an analysis of the error distribution for model validation indicated that the coupled model shows a more uniform distribution than the standalone model, as visualized in Fig. 3(c).

The stripping stage prediction from the loaded LIX 973 N was conducted to evaluate the collective interactions of input factors, namely H_2SO_4 concentration, temperature, duration, and A/O ratio, on Cu recovery. Among 90 data points, a random sample to train both models, comprising 80 % of the data, was utilized, while the remaining 20 % was reserved for model validation. The SVR model yielded MSE, RMSE, and R^2 values of 30.00, 5.47, and 0.96 for the training step, while the hybrid SVR-GWO model produced values of 5.72, 2.39, and 0.99, respectively. Fig. 4 shows the accuracy of the integrated model using a goodness-of-fit test, which considered metrics such as MSE, RMSE, mean, and Standard deviation (StD). The SVR model produced values of 52.94, 7.27, −4.01, and 6.24 for MSE, RMSE, mean, and StD, respectively, in the validation dataset of Cu stripping process. The validation dataset's poor metrics suggested that the SVR model failed to adapt to the training data during its learning phase. In contrast, when using the SVR-GWO model, the validation data yielded 7.88, 2.80, −1.29, and 2.56 values for the MSE, RMSE, mean, and StD, respectively. The SVR-GWO model can be considered a more resilient predictive model for Cu stripping projection owing to its significantly higher accuracy than the independent model. Table S2 delineates the hyperparameter values utilized in the predictive modeling and optimization of Cu reactive extraction data. The GWO optimizes the parameters of the SVR model by iteratively adjusting these

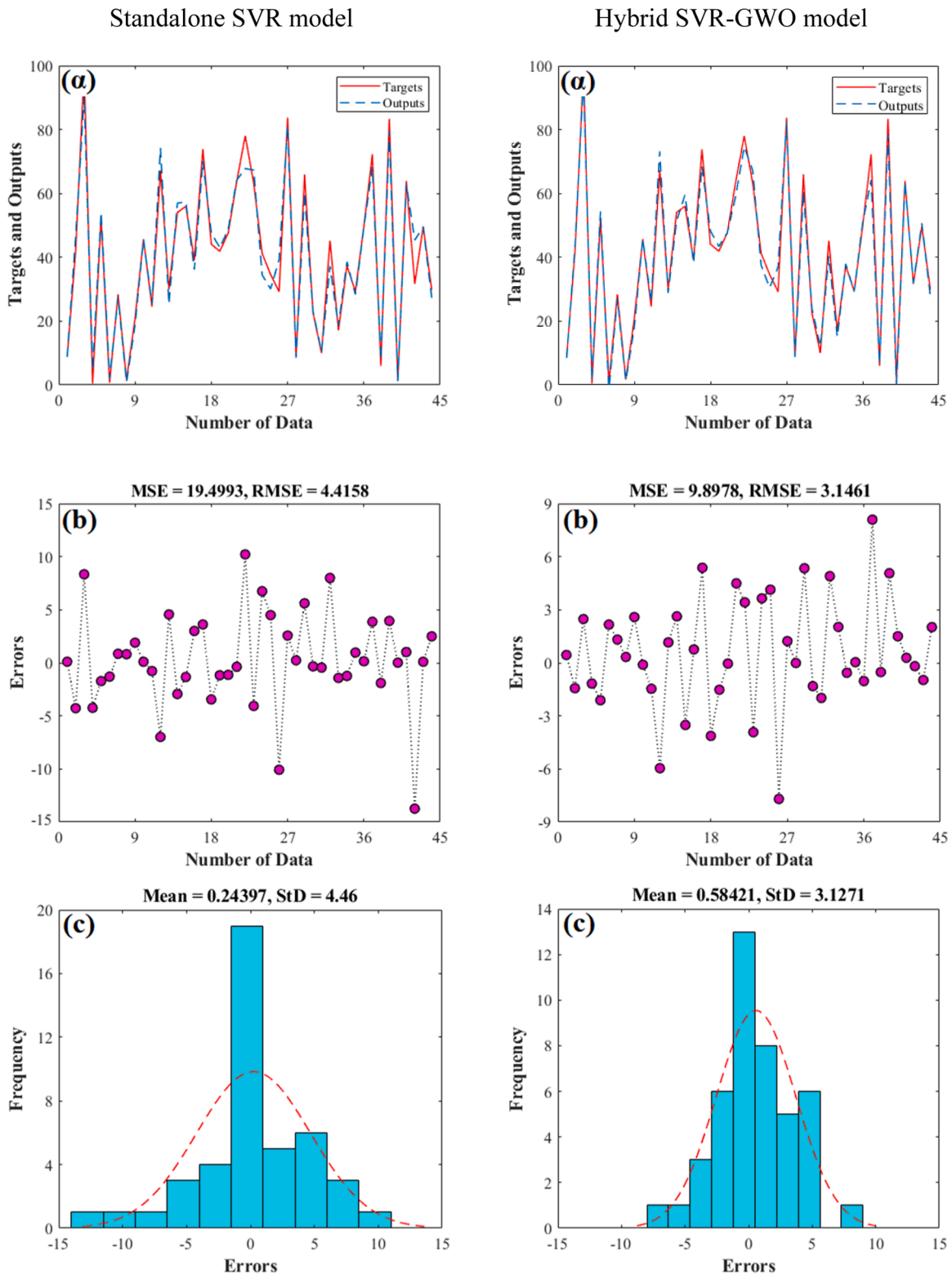

Fig. 2. Performance of models on the validation dataset of the copper leaching: a) Target and outputs; b) MSE and RMSE values; c) Frequency of errors.

parameters to minimize prediction and validation errors.

3.2. Models' uncertainty analysis

The values of independent variables were effectively validated according to the developed hybrid SVR-GWO model by integrating the PERT distribution function and pseudo-random numbers in Monte Carlo simulations (MCS). The histogram (Fig. 5(a)) depicts the probability density distribution of the Cu leaching efficiency, simulating values spanning from around −0.85–89.96, suggesting a notable diversity in the uncertainty. The simulation, performed over 10,000 iterations, yields a 90 % confidence interval for the predicted leaching efficiency between 39.33 and 39.82, demonstrating the model's strong capability in estimating the efficiency with a high degree of confidence. The

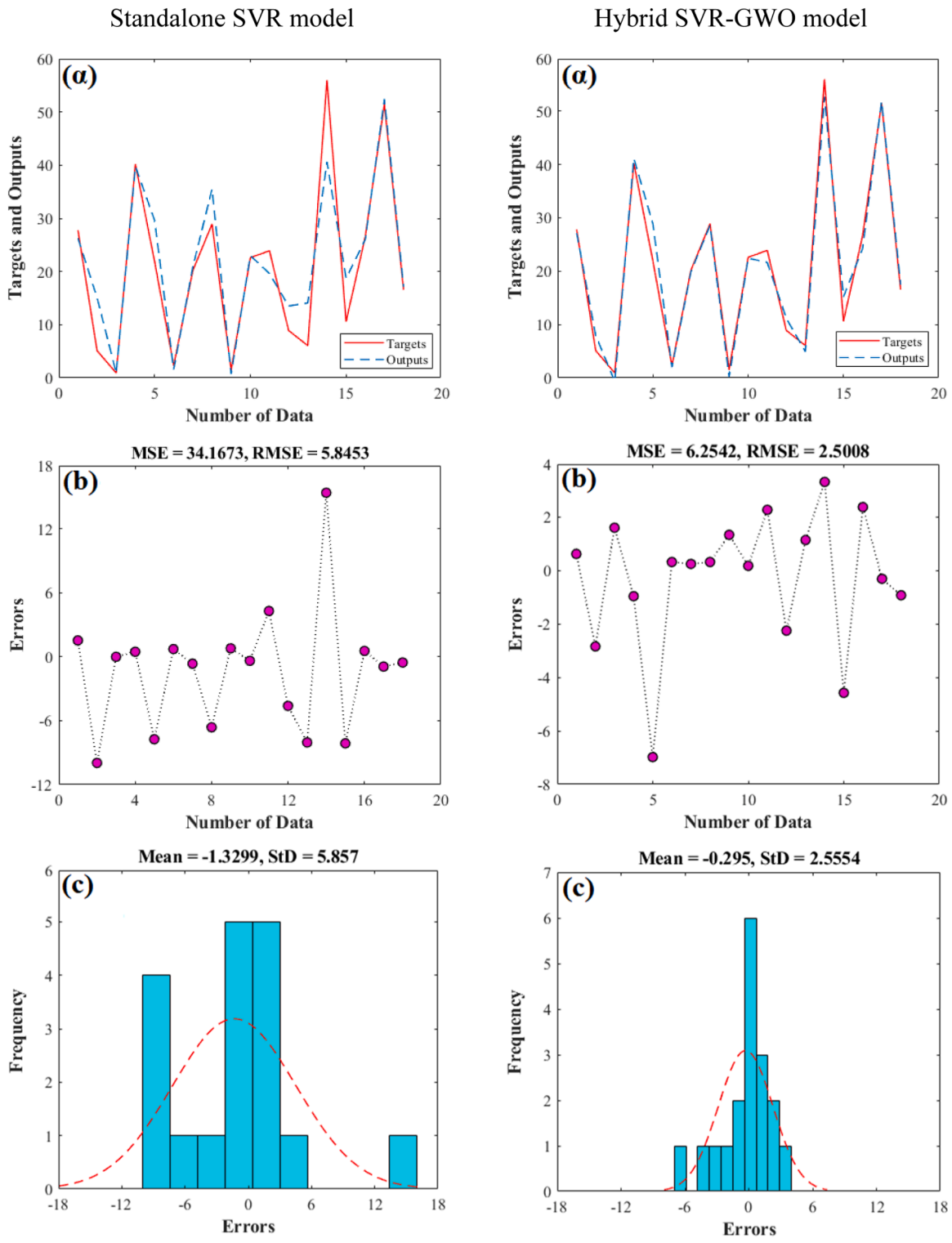

Fig. 3. Performance of models on the validation dataset of the copper extraction: a) Target and outputs; b) MSE and RMSE values; c) Frequency of errors.

statistical metrics suggest a moderately broad distribution characterized by a skewness of 0.16 and a kurtosis of 2.62, which indicates a slight positive skew and moderate tail behavior. Fig. 5(b), the uncertainty simulated histogram for extraction efficiency includes a mean value of 26.87 and a standard deviation of 12.15, suggesting a narrower distribution than the leaching efficiency. The distribution demonstrates a slight positive skewness of 0.44 and a kurtosis of 2.88 with a moderate departure from normality, characterized by relatively heavier tails. Fig. 5(c) presents the simulated uncertainty associated with the optimized hybrid model for copper stripping, with a mean stripping efficiency value of 70.45. The distribution ranged from 22.64 to 101.29, with a median value of 71.61 and a standard deviation of 14.91, indicating a considerable variability in the values derived from the stochastic model methodology. The distribution exhibits a minor negative skewness of −0.34, with the tail extending toward the lower range of the predicted values. Also, the kurtosis value of 2.47 suggests that the distribution's tails are similar to those found in a normal distribution, with a slight inclination towards platykurtosis. The leaching and extraction

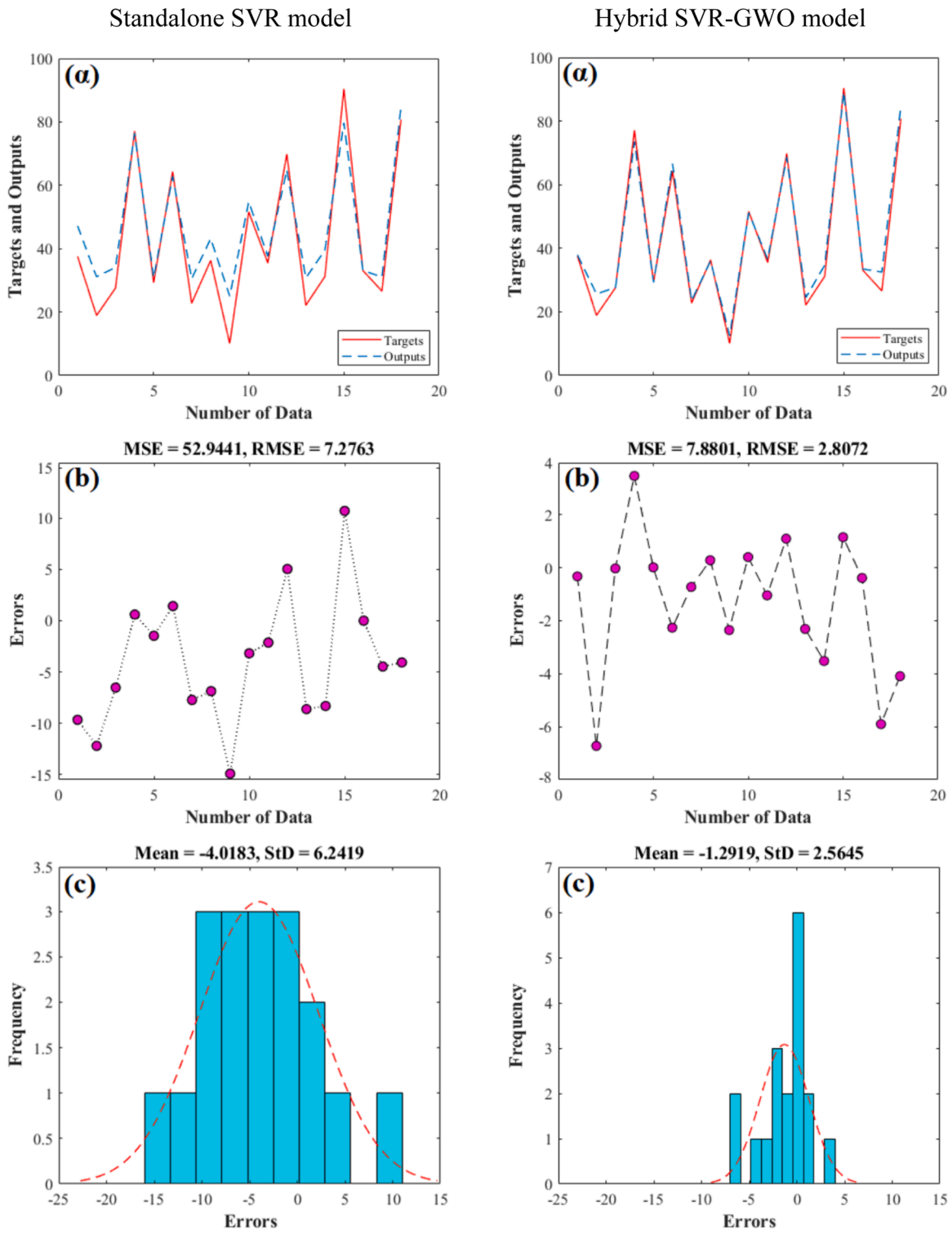

Fig. 4. Performance of models on the validation dataset of the copper stripping: a) Target and outputs; b) MSE and RMSE values; c) Frequency of errors.

processes exhibited greater consistency in their simulative outcomes, whereas the stripping process demonstrated notable variability and uncertainty.

3.3. Copper leaching process

The MLA was employed to optimize the interaction effects among all independent variables in leaching experiments, in contrast to previous studies that utilized the one-factor-at-a-time approach. In Fig. 6(a-c), the leaching efficiency of WPCBs was indicated by utilizing differing concentrations of HNO_3 while taking into account the collective impact of pulp density, temperature, and time. The coupled model prediction results of Cu leaching were found to be positively correlated with the concentration of HNO_3, demonstrating an increase in leaching as acid concentration increased. Under optimum conditions (with a 120 min time, 75°C temperature, and 7 % pulp density), this trend culminated in a recovery rate exceeding 96 % at an HNO_3 concentration of 4.0 M, after which efficiency experienced a slight decline with an increase in acid

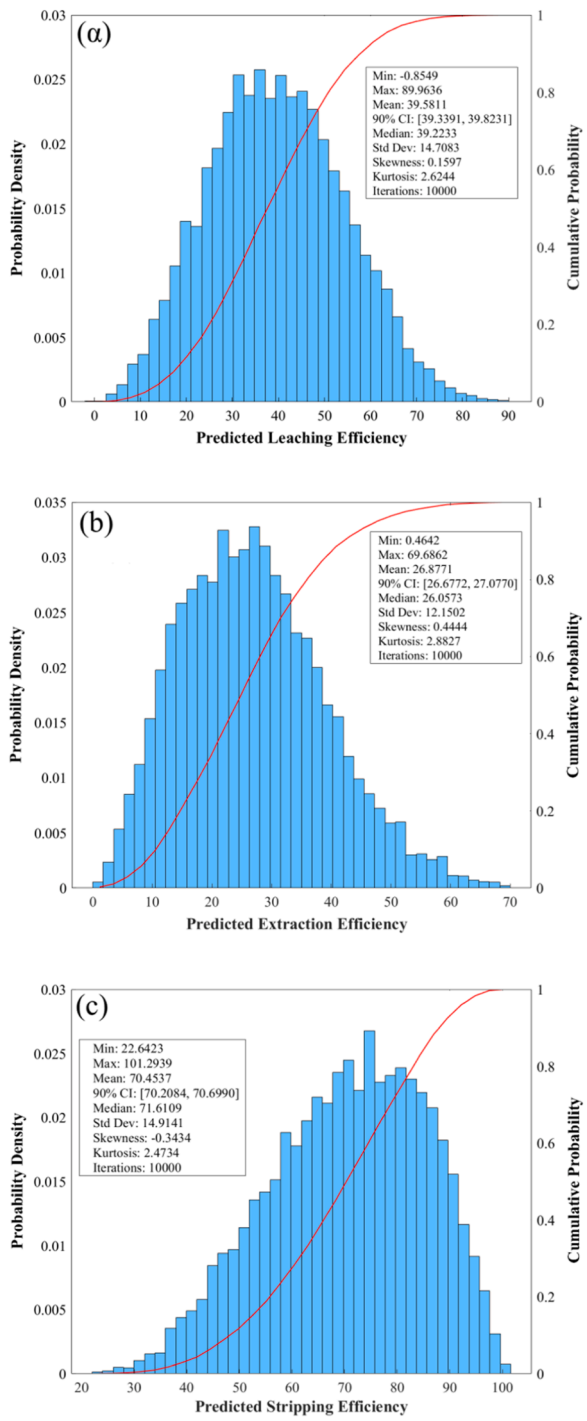

Fig. 5. Uncertainty analysis of independent parameters based-hybridized SVR-GWO model: (a leaching; b) extraction; c) stripping.

concentration to 5.0 M. The observed behavior may be attributed to an increase in nitrate ion concentration within the solution, as a greater concentration of acid aids in stabilizing surface oxide layers, thereby inhibiting the release of metal ions into the overall acidic solution. The overall reaction of Cu dissolution in the HNO_3 system can be represented by Eq. (18), wherein Cu reacts with HNO_3 to yield copper nitrate and nitrogen peroxide.

$$Cu + 4HNO_3 \rightarrow Cu^{2+} + 2NO_3^- + 2H_2O + 2NO_2 \quad (18)$$

The empirical data-based predicted results demonstrated that an increase in pulp density of up to 10 % resulted in a gradual decline in Cu leaching efficiency when subjected to prolonged leaching times or high temperatures. However, beyond this threshold, a substantial reduction in the leaching efficiency was observed at higher pulp densities ranging from 10 % to 20 %. The increased pulp densities lead to limited mass transfer, a phenomenon consistent with observations made by Chen and co-workers [31], and a reduction in residual acid concentration, as shown in the research by Panda and co-workers [32]. Fig. 6(b and d) indicate the correlation between the leaching of Cu and the reaction temperature concerning HNO_3 concentration and pulp density, respectively The hybrid approach found that the concurrent influence of temperature and HNO_3 concentration exerted a more pronounced effect on leaching efficiency than the interplay between temperature and pulp density. Specifically, as temperature increased across a range of acid concentrations, the resulting impact on the Cu leaching efficiency outweighed the effects of varying pulp densities. The findings showed that the temperature influence on Cu leaching is relatively minimal when it falls within the range of 15–35 °C. However, the heightened effect of temperature on the leaching reaction was observed within the range of 35–75 °C, leading to an escalation in the rate of reaction and decomposition of nitrate ions as the temperature was elevated within this interval. Fig. 6(c, e, and f) depicts the predicted data on Cu separation from WPCBs through leaching about the residence time. The output parameter prediction demonstrated an improvement in Cu recovery when the residence time increased. However, the rate of improvement began to slow down after the leaching time exceeded 100 min. According to the applied algorithm, the optimized time of 120 min was suggested to investigate the impact of system variables on the maximum efficiency of the recovery. Under the optimized point, the solution obtained from the leach experiments of WPCBs contained Cu, Fe, Al, Ni, Pb, and Sn concentrations of 23.96, 0.32, 0.40, 0.27, 0.13, and 0.05 g/L, respectively.

3.3.1. *Leaching kinetic study related to modeling data*

The shrinking core model and multiple reaction equations contribute to an increased depth and complexity in the leaching study [33]. The mathematical expressions obtained from these equations offer a quantitative depiction of the leaching kinetics, illuminating the underlying processes involved. These equations can be expressed as follows [34]:

$$1 - 3(1-x)^{2/3} + 2(1-x) = kt \text{Pore diffusion control} \quad (19)$$

$$1 - (1-x)^{1/3} = kt \text{Chemical reaction control} \quad (20)$$

$$x = kt \text{Fluid film diffusion control} \quad (21)$$

where, the fractional conversion, reaction time, and rate constant were assumed with x, t, and k variables, respectively. Based on Fig S2, the R^2 value for the chemical control reaction in the precise shrinking core model exhibited a near equivalence to unity, in contrast to the regression lines of other distinct equations. Consequently, the central region diminishes as the reaction progresses, while the surface reaction retains its predominant role in regulating the rate. The rate of reaction occurring at the interface of the solid and liquid phases consistently serves as the predominant constraining factor throughout most of the leaching process. Determining activation energy involves applying an Arrhenius equation, which accounts for the impact of temperature on the rate constant [35]. The data analysis in Fig S2(d) yielded an activation energy of 15.5 kcal/mol, consistent with the anticipated range of 10–25 kcal/mol for the chemically controlled model.

3.4. *HNO_3 recycling process*

Nitric acid is classified as a potent mineral acid with highly corrosive properties, and the unintended discharge of HNO_3 into the surrounding environment presents potential hazards to human, animal, and plant populations [36]. Furthermore, the reutilization of recycled HNO_3 from

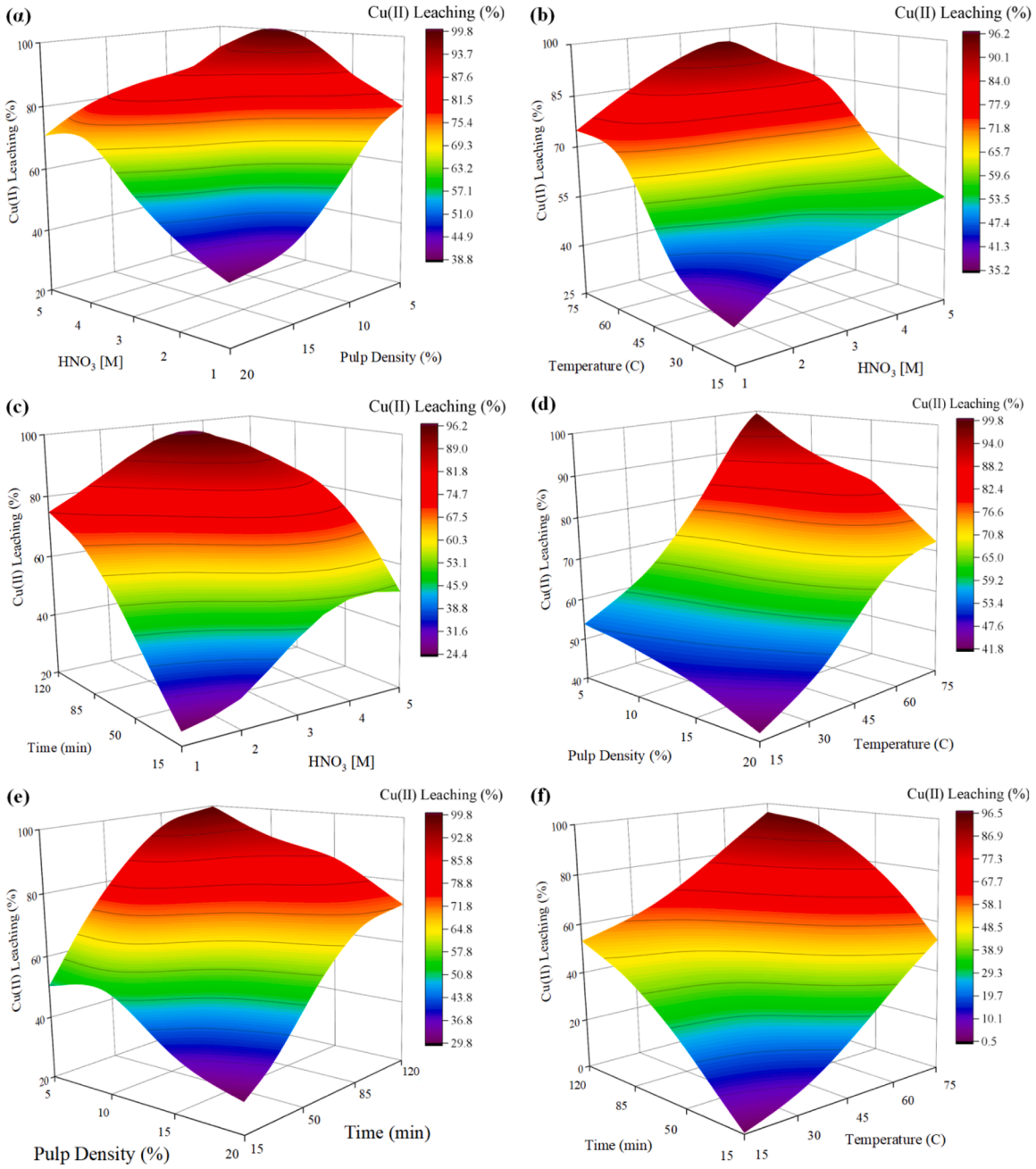

Fig. 6. The interactive impact of parameters on the copper leaching efficiency: a) HNO_3 and pulp density; b) HNO_3 and temperature; c) HNO_3 and time; d) pulp density and temperature; e) pulp density and time; f) time and temperature.

the obtained solution can be incorporated into the leaching process, reflecting a circular recycling approach to reduce reagent consumption. To achieve the best separation conditions, experiments were conducted to examine the effect of TBP concentration and the phase ratio on the recycling of HNO_3. The results depicted in Fig. 7(a) demonstrated that the extraction efficiency of nitric acid at ambient temperature enhanced from 20 % to 45.7 % during a single contact as the concentration of TBP elevated from 20 to 100 (v/v)% while maintaining an equivalent phase ratio. Utilizing the log-log plot to analyze the relationship between the distribution coefficient and the concentration of TBP under constant conditions enables the determination of the number of extractant molecules involved in forming the extracted acid complex. The indicated slope of 0.76 in Fig. 7(b) suggested that a stoichiometric ratio of one mole of TBP was required to extract one mole of HNO_3 from the leach liquor of WPCBs. Hence, the extraction of HNO_3 using TBP can be explained through the hydrate-solvate mechanism [37], with the extraction process being represented by the following reaction:

$$[TBP]_{(org)} + [HNO_3]_{(aq)} \rightarrow [TBP \bullet HNO_3 \quad]_{(org)} \tag{22}$$

Based on Fig. 7(c), the impact of HNO_3 recycling from waste acid solution was observed to increase from 20.1 % to 62.8 % with variations in O/A ratio within the range of 0.25–3.0, utilizing concentrated TBP at ambient temperature for 15 min. The McCabe-Thiele plot was constructed to ascertain the theoretical number of stages necessary for the quantitative extraction of nitric acid, with results delineated in Fig. 7(d). The extraction isotherm analysis revealed that near-complete recycling of nitric acid could be attained in four sequential stages at an O/A ratio of 3, as corroborated by counter-current experimentation. During the back-extraction operation, deionized water was employed for HNO_3 recovery from the loaded organic phase. A nearly complete HNO_3

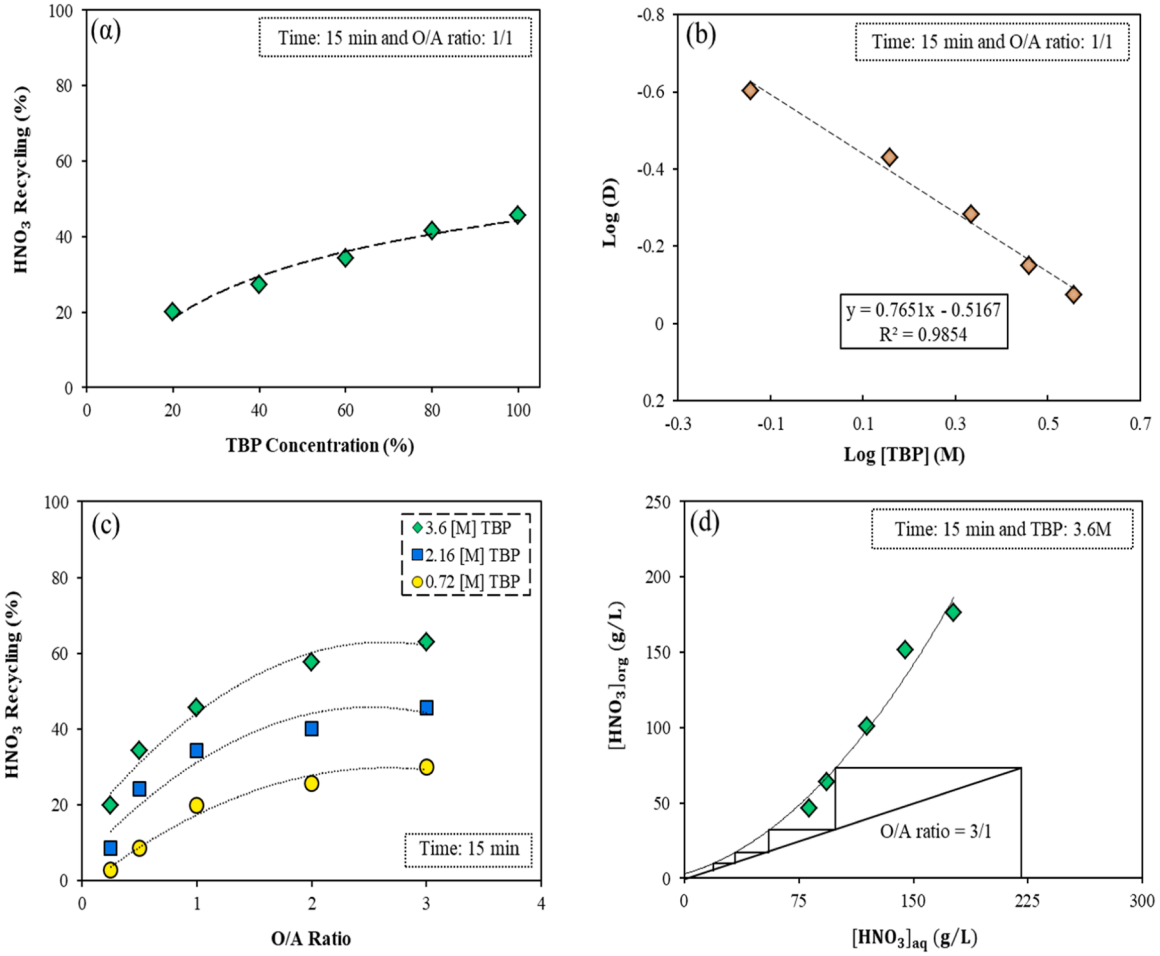

Fig. 7. Investigation of HNO_3 recycling from the leaching solution: a) impact of TBP concentration; b) Log (D) vs. Log [TBP]; c) impact of different phase ratio; d) McCabe-Thiele diagram.

recovery was accomplished by implementing a five-stage counter-current process, utilizing an equal phase ratio, as illustrated in Fig S3.

3.5. Copper extraction process

The decrease in volume due to acid recycling for future leaching experiments led to changes in the leach solution of WPCBs, resulting in increased concentrations of Cu, Fe, Al, Ni, Pb, and Sn, measuring 31.80, 0.42, 0.52, 0.32, 0.17, and 0.07 g/L, respectively. The process of purifying and recycling Cu from impurities involved using a liquid–liquid extraction method by employment of LIX973N. By fine-tuning hyperparameters of the SVR model with the GWO, the optimal performance for Cu extraction process was determined at an equilibrium pH of 2.5, extractant concentration of 30 %(v/v), 20 min contact time, and equal phase ratio. The developed model predicted an extraction efficiency of 73.0 % from the leaching solution. Fig. 8(a) is a 3D surface plotted by Origin software demonstrating the impact of equilibrium pH and LIX 973 N concentration on the Cu extraction yield under fixed conditions with the same phase ratio for 20 min. The efficiency Cu at different equilibrium pH ranges from 0.5 to 2.5 versus 30 % (v/v) LIX973N indicated an increase in the efficiency from 4.5 to 73.0. Based on the Eh–pH diagram for the Cu-H_2O system at ambient temperature, the predominant copper species present at acidic pH values are observed as Cu^{2+} and Cu^{+} [38]. The successful separation of copper using LIX 973 N can be attributed to the specific copper species present within the equilibrium pH range of 2–2.5. Sridhar and Verma also observed similar results when they conducted experiments on extracting copper from aqueous solutions using LIX 984 N [39]. Their findings revealed that the efficiency of Cu extraction significantly rose from 15 % to 98 % as the solution pH increased from 0.5 to 3.0. Fig. 8(a-b) shows the impact of the interactions of LIX 973 N with Cu. As the concentration of the extractant increased, the efficiency of extracting Cu from the leach solution also increased. This behavior can be attributed to more solvent molecules being available for Cu extraction. The impact of the contact time on the yield of Cu extraction is shown in Fig. 8(c). The output data revealed an increase in Cu extraction from 63.7 to 73 with an increase in contact time from 5 to 20 min while maintaining a constant concentration of LIX 973 N at 30 % and an O/A phase ratio of 1. Fig. 8(d) presents the modeling results concerning extraction behavior as a function of varying phase ratios and equilibrium pH values. The data indicate a predicted optimal point of 73.0 %, attained at an equal phase ratio and an equilibrium pH of 2.5. The extraction isotherm results, which determine the necessary number of theoretical stages for achieving complete recovery under specific conditions, were predicted using the combined model at various O/A ratios ranging from 0.2 to 2 under optimized points. The predicted data employing the SVR-GWO model and further aided by the McCabe-Thiele diagram determined that four counter-current extraction stages were needed to extract almost entirely metal (Fig S4).

3.6. FTIR analysis on organic phase and Cu-loaded LIX973N

The FT-IR technique has been widely employed in the analysis of bonding within metal-organic complexes, providing essential information on reaction mechanisms and the structural characteristics of such

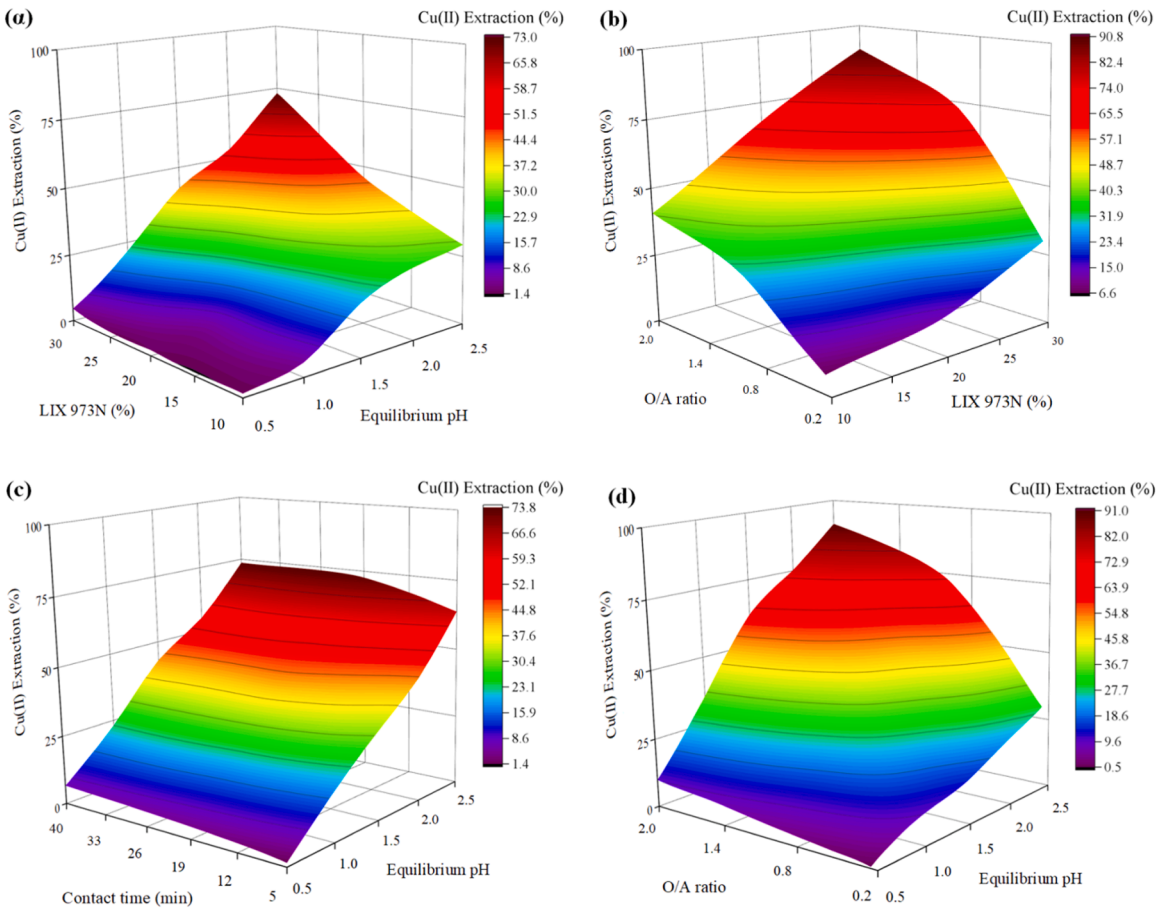

Fig. 8. The interactive impact of parameters on the copper extraction efficiency: a) LIX 973 N and equilibrium pH; b) LIX 973 N and O/A ratio; c) equilibrium pH and contact time; d) equilibrium pH and O/A ratio.

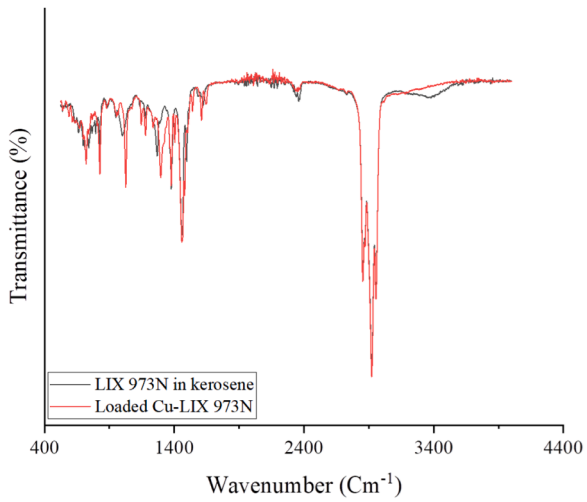

Fig. 9. The infrared spectra of LIX973N in Kerosene and the loaded organic phase.

metal complexes [40]. The comparative analysis of the spectra corresponding to the organic phase composed of LIX973N and kerosene, as well as the spectrum of the Copper-LIX973N complex, is shown in Fig. 9. The organic phase analysis indicates that the O-H stretching band around 3400 cm^{-1} is due to the hydroxide group found in the oxime. The oxime groups' existence in LIX 973 N leads to peaks in the 1600–1700 cm^{-1} range associated with C═N Stretching vibration. Moreover, the oxime functional group is characterized by a C═N-OH structural framework, where the stretching vibration of the C-N band may manifest in the wavenumber range of 1000–1200 cm^{-1}. The C-H stretching modes were observed as pronounced peaks in the 2850–2950 cm^{-1} range, characteristic of aliphatic hydrocarbons. Besides, the C-H bending vibrations manifested as peaks in the 1350–1450 cm^{-1} spectral range, indicating the presence of hydrocarbon compounds. A comparison of the infrared spectra of the Cu-LIX 973 N complex with that of LIX973N in isolation revealed that the interaction between Cu and the hydroxyl, as well as oxime groups, resulted in alterations or shifts in the intensity of the O-H stretching vibrations observed at 3400 cm^{-1}. A significant alteration in the C═N stretching region indicates the development of a copper-oxime complex. This complexation generally shifts towards lower wavenumbers, reflecting modifications in the electronic environment surrounding the C═N band. Also, the observed alteration in the transmission band at around 1010 cm^{-1} can be attributed to the Cu-O band or interaction, signifying changes in the metal-ligand coordination sphere.

3.7. Copper stripping process

Cu was stripped from a loaded organic solution using H2SO4 as a stripping agent to achieve copper sulfate salt. The response surface plotted by the software in Fig. 10 (a–d) illustrates the correlation between the input and target variables in three dimensions. The integrated model estimated the stripping yield of 73.6 % in the optimum condition, with a respective H_2SO_4 concentration of 2 M and the A/O ratio of 0.3 for 20 min at ambient temperature. The increase in the stripping process's efficiency was linked to the simultaneous enhancement in the

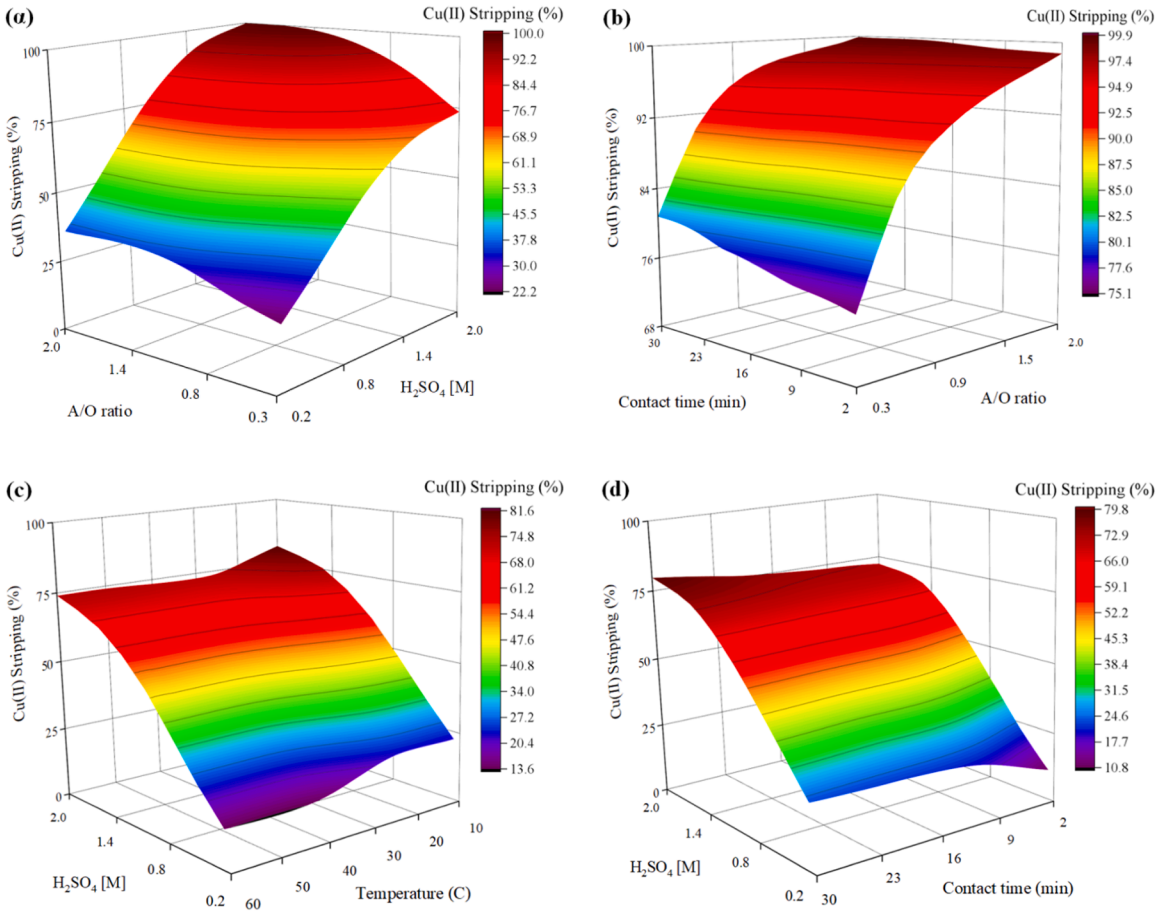

Fig. 10. The interactive impact of parameters on the copper stripping efficiency: a) H_2SO_4 and A/O ratio; b) contact time and A/O ratio; c) H_2SO_4 and temperature; d) H_2SO_4 and contact time.

concentration of the stripping reagent, which improved the reactivity between copper and sulfate ions. The reduction in reaction temperature alongside an extension in contact time demonstrated a beneficial impact on the Cu stripping process. Similarly, enhancing the A/O ratio resulted in improved process efficiency. Consequently, the optimal conditions for recovering copper from the loaded LIX 973 N phase involved a lower temperature, higher A/O ratio, and extended mixing time. However, considering the significance of cost savings in industrial settings and the negligible effect of temperature on the stripping process, the room temperature was the most favorable. In addition, the MLA outcomes predicted that a contact time of 20 min proved sufficient to attain an equilibrium state. The necessary number of counter-current stages in the Cu stripping process was determined by applying the SVR-GWO results to the McCabe-Thiele diagram, utilizing the predicted phase variation data. Fig S5 shows that at an A/O ratio of 0.3, three theoretical stages were necessary to achieve nearly complete stripping, and an approximately threefold increase in Cu enrichment, reaching 104 g/L, was attainable under optimized conditions.

3.8. Morphology and phase analysis

Fig. 11 depicts the XRD pattern obtained from the crystallized Cu sample under the optimized condition, revealing varying relative intensities of the dominant peaks. The appearance of the $CuSO_4$ phase offers promising prospects as a precursor for the fabrication of innovative electronic devices. The samples exhibit a crystalline arrangement, and the distinctive peaks at 2θ values of 18.4, 25.9, 26.3, 28.4, and 36.2 are indicative of their pattern. These observed peaks can be attributed to the copper sulfate phases [41]. The copper sulfate product underwent SEM analysis at various scales to illustrate surface morphology and topography data. The images revealed the presence of considerably large near-crystal particles. Copper and impurities were also reclaimed, and the results are outlined in Table S2, highlighting the promising potential for copper reclamation at a purity level of up to 99.7 %.

4. Conclusions

This study conducted a comprehensive experimental analysis of the interactive impacts of operational parameters and performance prediction on Cu reclamation from WPCBs from hydrometallurgy aspects for the first time using the hybrid ML approach. SVR-GWO modeling was a powerful decision-support tool for deciphering intricate connections among system variables, including copper separation from WPCBs, which is crucial for ensuring the sustainable development and effective management of waste resources. The leaching modeling findings demonstrated 96.1 % Cu efficiency when the optimal process parameters, such as HNO_3 concentration, pulp density, temperature, and duration, were determined to be 4 M, 7 %, 75 °C, and 2 h, respectively. TBP, as a solvent, to facilitate the recycling of nitric acid from the leach liquor of PCBs presented a viable solution to the ecological challenges posed by the processing industry while enabling a more favorable lower concentration of HNO_3 for downstream separations through liquid–liquid extraction. The McCabe-Thiele plot indicated that undiluted TBP could attain recycling in four theoretical stages with an O/A ratio of 3 for 15 min. The behavior prediction of Cu separation from an acid-free leaching solution obtained utilizing LIX 973 N was analyzed by standalone and hybrid SVR models. The validated model confirmed the experimental findings by quantitatively verifying the recovery of Cu at

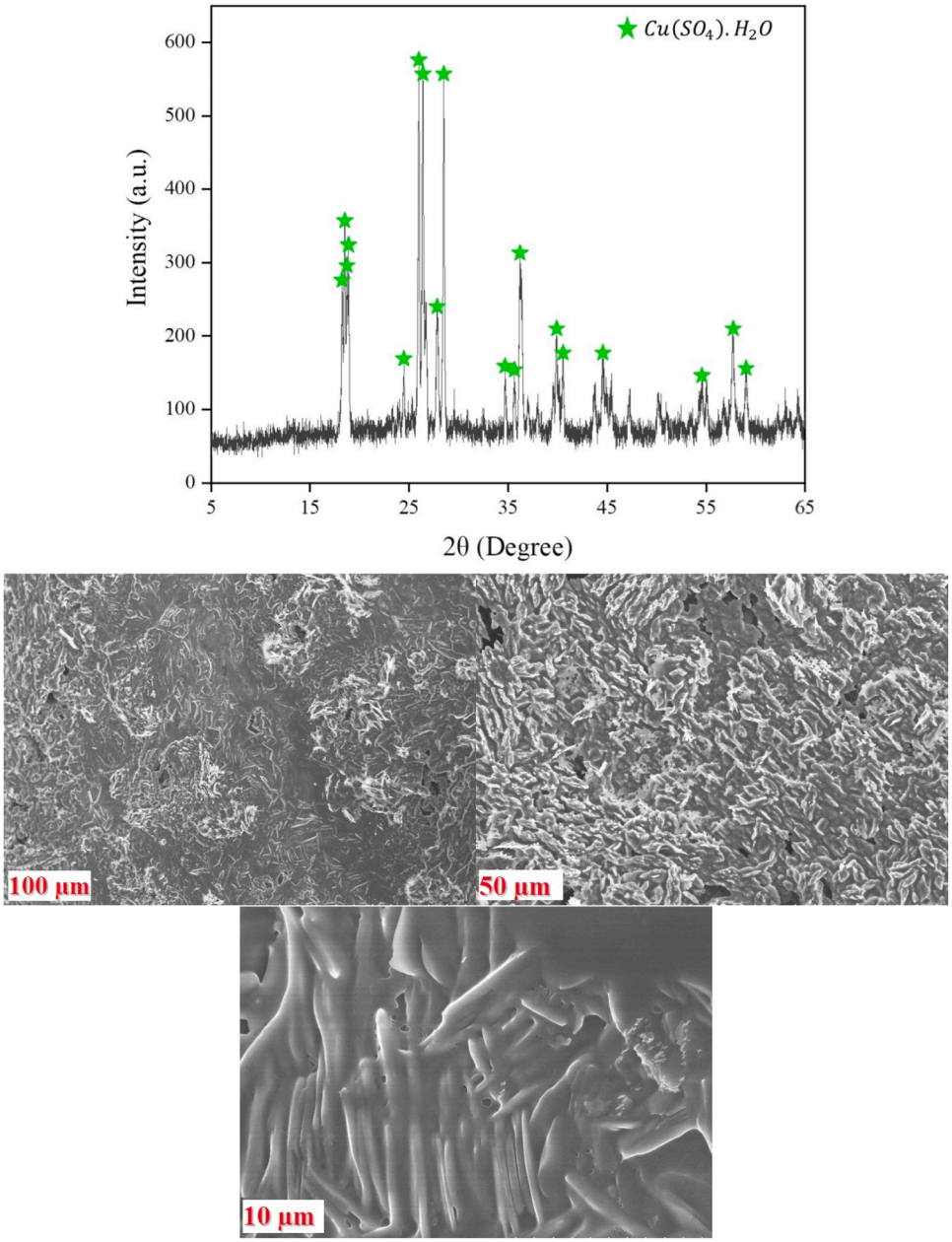

Fig. 11. XRD and SEM analysis of the final product of crystallized copper sulfate.

optimum conditions, including an equilibrium pH of 2.5, 30 % extractant concentration, 20 min time, and equal phase ratio. The isotherm data, predicted using the model and complemented by the McCabe-Thiele diagram, indicated that four counter-current stages were required to achieve nearly complete extraction. The developed model optimized the stripping process by applying 2 M H_2SO_4 as the stripping agent with a 0.3 A/O ratio at 25 °C for 20 min. In the models' validation stages, the performance of the coupled model surpassed that of the standalone SVR model, as evidenced by the lower values of MSE observed in the leaching, extraction, and stripping stages, which were 9.89, 6.25, and 7.87, respectively. Finally, the effectiveness of the optimized hydrometallurgical process for copper reclamation was substantiated by applying XRD and SEM analyses. The experimental data uncertainty analysis using MCS, with 10,000 iterations, demonstrated the robustness and reliability of the SVR-GWO model, reinforcing its credibility as a decision-support tool for sustainable e-waste management.

CRediT authorship contribution statement

Jin Young Lee: Supervision, Resources, Project administration, Funding acquisition. **Amir Razmjou:** Formal analysis. **Rajesh Kumar Jyothi:** Formal analysis. **Martina Petranikova:** Writing – review & editing, Supervision, Formal analysis, Conceptualization. **Mehdi Khiadani:** Writing – review & editing, Formal analysis. **Hee-Nam Kang:** Writing – original draft, Visualization, Formal analysis. **Benyamin Shakib:** Writing – original draft, Validation, Software, Methodology, Investigation, Data curation, Conceptualization.

Declaration of Competing Interest

The authors declare that they have no known competing financial interests or personal relationships that could have appeared to influence the work reported in this paper.

Data availability

Data will be made available on request.

Acknowledgment

This work was supported by the Korea Institute of Energy Technology Evaluation and Planning (KETEP) grant funded by the Korean government (MOTIE) (20217510100020, Development of a platform process using a common core and materialization technology for rare metal recovery from industrial low-grade waste liquid). The authors would like to extend their deepest gratitude to the three unidentified reviewers for their valuable input, consisting of perceptive feedback and considerate suggestions, which have greatly enhanced the academic quality of the paper.

Appendix A. Supporting information

Supplementary data associated with this article can be found in the online version at doi:10.1016/j.jece.2024.114056.

References

[1] O.S. Shittu, I.D. Williams, P.J. Shaw, Global E-waste management: can WEEE make a difference? A review of e-waste trends, legislation, contemporary issues and future challenges, Waste Manag. 120 (2021) 549–563.
[2] A. Kumar, M. Holuszko, D.C.R. Espinosa, E-waste: an overview on generation, collection, legislation and recycling practices, Resour., Conserv. Recycl. 122 (2017) 32–42.
[3] S. Mir, N. Dhawan, A comprehensive review on the recycling of discarded printed circuit boards for resource recovery, Resour., Conserv. Recycl. 178 (2022) 106027.
[4] P. Hadi, M. Xu, C.S. Lin, C.-W. Hui, G. McKay, Waste printed circuit board recycling techniques and product utilization, J. Hazard. Mater. 283 (2015) 234–243.
[5] A. Işıldar, E.R. Rene, E.D. van Hullebusch, P.N. Lens, Electronic waste as a secondary source of critical metals: management and recovery technologies, Resour., Conserv. Recycl. 135 (2018) 296–312.
[6] A. Alengebawy, S.T. Abdelkhalek, S.R. Qureshi, M.-Q. Wang, Heavy metals and pesticides toxicity in agricultural soil and plants: ecological risks and human health implications, Toxics 9 (2021) 42.
[7] P.P. Leal, C.L. Hurd, S.G. Sander, E. Armstrong, P.A. Fernández, T.J. Suhrhoff, M. Y. Roleda, Copper pollution exacerbates the effects of ocean acidification and warming on kelp microscopic early life stages, Sci. Rep. 8 (2018) 14763.
[8] J. Cui, L. Zhang, Metallurgical recovery of metals from electronic waste: a review, J. Hazard. Mater. 158 (2008) 228–256.
[9] Y. Lu, Z. Xu, Precious metals recovery from waste printed circuit boards: a review for current status and perspective, Resour., Conserv. Recycl. 113 (2016) 28–39.
[10] A. Liu, G. Hu, Y. Wu, F. Guo, Life cycle environmental impacts of pyrometallurgical and hydrometallurgical recovery processes for spent lithium-ion batteries: present and future perspectives, Clean. Technol. Environ. Policy 26 (2024) 381–400.
[11] I. Tezyapar Kara, K. Kremser, S. Wagland, F. Coulon, Bioleaching metal-bearing wastes and by-products for resource recovery: a review, Environ. Chem. Lett. 21 (2023) 3329–3350.
[12] K.N. Han, R. Kim, J. Kim, Recent advancements in hydrometallurgy: solubility and separation, Trans. Indian Inst. Met. (2023) 1–13.
[13] O.S. Dinkar, R. Panda, P.K. Choubey, M.K. Jha, B. Ambade, Studies on the hydrometallurgical recovery of metals from used and end of life PCBs, in: TMS Annual Meeting & Exhibition, Springer, 2023, pp. 83-94.
[14] A.D. Bas, H. Deveci, E.Y. Yazici, Treatment of manufacturing scrap TV boards by nitric acid leaching, Sep. Purif. Technol. 130 (2014) 151–159.
[15] G. Ji, Y. Liao, Y. Wu, J. Xi, Q. Liu, A review on the research of hydrometallurgical leaching of low-grade complex chalcopyrite, J. Sustain. Metall. 8 (2022) 964–977.
[16] C.J. Oh, S.O. Lee, H.S. Yang, T.J. Ha, M.J. Kim, Selective leaching of valuable metals from waste printed circuit boards, J. Air Waste Manag. Assoc. 53 (2003) 897–902.
[17] M.D. Rao, K.K. Singh, C.A. Morrison, J.B. Love, Recycling copper and gold from e-waste by a two-stage leaching and solvent extraction process, Sep. Purif. Technol. 263 (2021) 118400.
[18] H. Yang, J. Liu, J. Yang, Leaching copper from shredded particles of waste printed circuit boards, J. Hazard. Mater. 187 (2011) 393–400.
[19] I. Birloaga, I. De Michelis, F. Ferella, M. Buzatu, F. Vegliò, Study on the influence of various factors in the hydrometallurgical processing of waste printed circuit boards for copper and gold recovery, Waste Manag. 33 (2013) 935–941.
[20] M. Kumar, J.-c Lee, M.-S. Kim, J. Jeong, K. Yoo, Leaching of metals from waste printed circuit boards (wpcbs) using sulfuric and nitric acids, Environ. Eng. Manag. J. (EEMJ) 13 (2014).
[21] Y. Sewsynker-Sukai, F. Faloye, E.B.G. Kana, Artificial neural networks: an efficient tool for modelling and optimization of biofuel production (a mini review), Biotechnol. Biotechnol. Equip. 31 (2017) 221–235.
[22] M.R. Dobbelaere, P.P. Plehiers, R. Van de Vijver, C.V. Stevens, K.M. Van Geem, Machine learning in chemical engineering: strengths, weaknesses, opportunities, and threats, Engineering 7 (2021) 1201–1211.
[23] S. Kumari, R. Panda, R. Prasad, R.D. Alorro, M.K. Jha, Sustainable Process to Recover Metals from Waste PCBs Using Physical Pre-Treatment and Hydrometallurgical Techniques, Sustainability 16 (2024) 418.
[24] V. Vapnik, The nature of statistical learning theory, Springer science & business media, 1999.
[25] H. Drucker, C.J. Burges, L. Kaufman, A. Smola, V. Vapnik, Support vector regression machines, Adv. Neural Inf. Process. Syst. 9 (1996).
[26] V.N. Vapnik, Adaptive and learning systems for signal processing communications, and control, Statistical learning theory, (1998).
[27] S. Kavitha, S. Varuna, R. Ramya, A comparative analysis on linear regression and support vector regression, in: 2016 online international conference on green engineering and technologies (IC-GET), IEEE, 2016, pp. 1-5.
[28] S. Mirjalili, S.M. Mirjalili, A. Lewis, Grey wolf optimizer, Adv. Eng. Softw. 69 (2014) 46–61.
[29] X. Wang, C. Su, N. Wang, H. Shi, Gray wolf optimizer with bubble-net predation for modeling fluidized catalytic cracking unit main fractionator, Sci. Rep. 12 (2022) 7548.
[30] A. Sahoo, S. Chandra, Multi-objective grey wolf optimizer for improved cervix lesion classification, Appl. Softw. Comput. 52 (2017) 64–80.
[31] M. Chen, J. Huang, O.A. Ogunseitan, N. Zhu, Y.-m Wang, Comparative study on copper leaching from waste printed circuit boards by typical ionic liquid acids, Waste Manag. 41 (2015) 142–147.
[32] R. Panda, S. Mishra, K.K. Pant, T. Bhaskar, S.N. Naik, A closed loop recycling strategy for sustainable recovery of group 11 metals (Cu, Au, and Ag) from waste PCBs: An amalgamation of low-temperature NH4Cl roasting, HCl leaching and cementation, Sustainable Materials and Technologies, (2023) e00652.
[33] M. Jung, B. Mishra, Kinetic and thermodynamic study of aluminum recovery from the aluminum smelter baghouse dust, J. Sustain. Metall. 2 (2016) 257–264.
[34] H. Lee, B. Mishra, Selective recovery and separation of copper and iron from fine materials of electronic waste processing, Miner. Eng. 123 (2018) 1–7.
[35] K.J. Laidler, The development of the Arrhenius equation, J. Chem. Educ. 61 (1984) 494.
[36] I. Shaw, J. Chadwick, Principles of environmental toxicology, CRC Press, 2018.
[37] P.K. Choubey, R. Panda, M.K. Jha, J.-c Lee, D. Pathak, Recovery of copper and recycling of acid from the leach liquor of discarded Printed Circuit Boards (PCBs), Sep. Purif. Technol. 156 (2015) 269–275.
[38] N. Takeno, Atlas of Eh-pH diagrams, Geol. Surv. Jpn. Open file Rep. 419 (2005) 285.
[39] V. Sridhar, J. Verma, Recovery of copper, nickel and zinc from sulfate solutions by solvent extraction using LIX 984N, E-J. Chem. 8 (2011) S434–S438.
[40] A. Dutta, Fourier transform infrared spectroscopy, Spectrosc. Methods Nanomater. Charact. (2017) 73–93.
[41] G. Shi, L. Wen, S. Zhang, J. Cheng, X. Chen, Y. Zhou, Z. Xu, B. Xin, Facile manufacture of high-purity CuSO4 from waste Cu-containing paint residue using combined processes of H2SO4 leaching and extraction stripping, Water Sci. Technol. 88 (2023) 2974–2985.
[42] E. Allahkarami, B. Rezai, R.R. Karri, N.M. Mubarak, Predictive capability evaluation and mechanism of Ce (III) extraction using solvent extraction with Cyanex 572, Sci. Rep. 12 (2022) 10379.
[43] M. Fan, J. Hu, R. Cao, K. Xiong, X. Wei, Modeling and prediction of copper removal from aqueous solutions by nZVI/rGO magnetic nanocomposites using ANN-GA and ANN-PSO, Sci. Rep. 7 (2017) 18040.
[44] N. Marchitan, C. Cojocaru, A. Mereuta, G. Duca, I. Cretescu, M. Gonta, Modeling and optimization of tartaric acid reactive extraction from aqueous solutions: a comparison between response surface methodology and artificial neural network, Sep. Purif. Technol. 75 (2010) 273–285.
[45] G. Sodeifian, S.A. Sajadian, N.S. Ardestani, Evaluation of the response surface and hybrid artificial neural network-genetic algorithm methodologies to determine extraction yield of Ferulago angulata through supercritical fluid, J. Taiwan Inst. Chem. Eng. 60 (2016) 165–173.
[46] D.N. Kartic, B.C.A. Narayana, M. Arivazhagan, Removal of high concentration of sulfate from pigment industry effluent by chemical precipitation using barium chloride: RSM and ANN modeling approach, J. Environ. Manag. 206 (2018) 69–76.
[47] J. Kabuba, M. Banza, Ion-exchange process for the removal of Ni (II) and Co (II) from wastewater using modified clinoptilolite: modeling by response surface methodology and artificial neural network, Results Eng. 8 (2020) 100189.
[48] H.Kamran Haghighi, D. Moradkhani, M. Salarirad, Modeling of synergetic effect of LIX 984N and D2EHPA on separation of iron and zinc using artificial neural network, Trans. Indian Inst. Met. 67 (2014) 331–341.
[49] N. Parveen, S. Zaidi, M. Danish, Development of SVR-based model and comparative analysis with MLR and ANN models for predicting the sorption capacity of Cr (VI), Process Saf. Environ. Prot. 107 (2017) 428–437.
[50] J. Pazhoohan, H. Beiki, M. Esfandyari, Experimental investigation and adaptive neural fuzzy inference system prediction of copper recovery from flotation tailings by acid leaching in a batch agitated tank, Int. J. Miner., Metall., Mater. 26 (2019) 538–546.
[51] N.G. Turan, O. Ozgonenel, The design and implementation of adsorptive removal of Cu (II) from leachate using ANFIS, Sci. World J. 2013 (2013).
[52] M. banza, T. Seodigeng, H. Rutto, Comparison Study of ANFIS, ANN, and RSM and mechanistic modeling for chromium (VI) removal using modified cellulose nanocrystals–sodium alginate (CNC–Alg), Arab. J. Sci. Eng. (2023) 1–19.